Refined Load Rating Analysis and Load Testing (MP 28.9 over the Garden State Parkway)

10 July 2012

Introduction

The purpose of this report is to document the activities and findings associated with the refined load rating and load testing of the MP 28.9 Bridge that crosses the Garden State Parkway in Atlantic County, NJ. Prior to this project, this bridge was rated using conventional approaches and it was determined that certain ratings factors were below 1.0. The goal of the project reported herein was to develop more accurate load rating factors through the integrated use of simulation models and sensing technologies. To guide this application, the process of structural identification (St-Id) shown in Figure 1 was followed rigorously. This approach is considered the most definitive method available to understand the performance of structures by combining engineering heuristics, simulation modeling, and sensing applications.

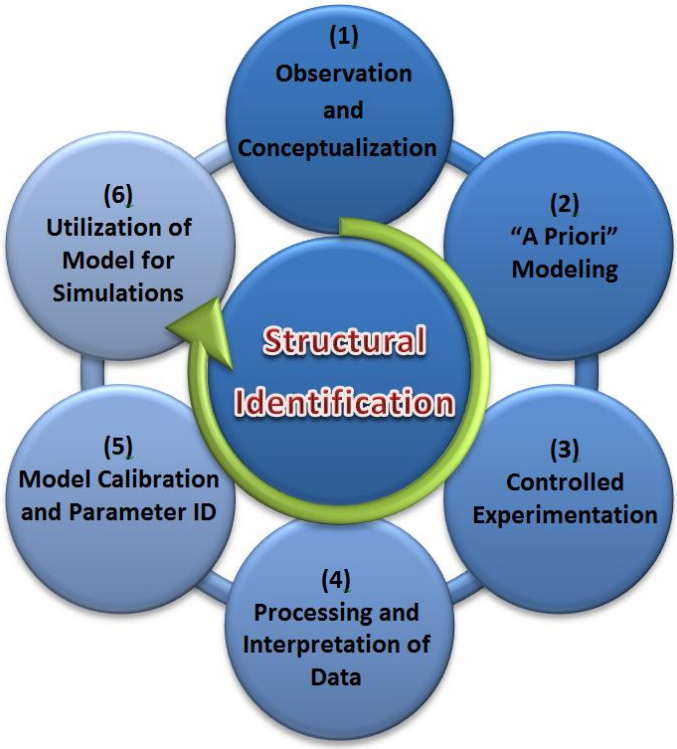

Figure 1 *– Structural Identification Process*

The following sections provide an overview of (a) the various steps taken to conceptualize the structure and its potential deficiencies, (b) the development of a 3D finite element (FE) model and the subsequent refined load rating analysis, (c) the design of a testing program to validate the FE model, (d) the execution of the testing program, (e) a comparison between the measured results and the FE model,

and (f) the development of rating factors for a series of construction vehicles and recommendations for future load rating analysis of the MP28.9 Bridge.

Observation and Conceptualization

The MP 28.9 Bridge carries Route 9 over the Garden State Parkway in southern Atlantic County, NJ (Figure 2). The bridge is comprised of four simply-supported, multi-girder steel stringer spans that are constructed from welded plate girders. The bridge has two relatively short approach spans of 42 ft. and 53 ft. and two relatively long center spans of 147 ft. with all spans having a skew angle of 49 degrees. The six welded plate girders that support the longer spans were designed to act compositely with the deck. To save on material costs, the girders were designed with flange thickness transitions. The girders are connected transversely through X-type diaphragms. The bridge also includes wind bracing that spans from the exterior girders across two bays to the interior girder on each side of the bridge, as seen in Figure 3.

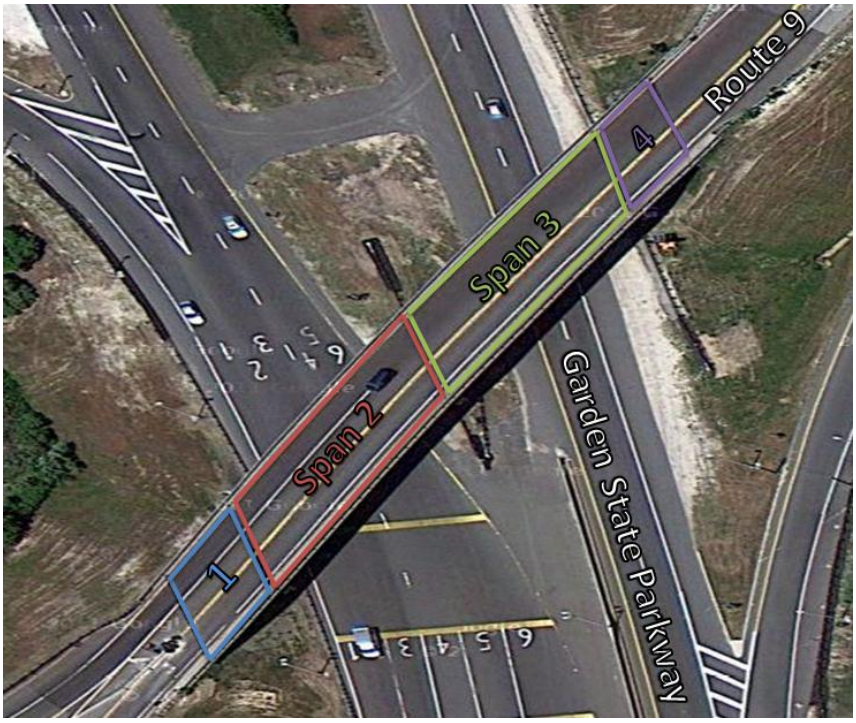

Figure 2 - *Arial photograph of the MP 28.9 Bridge*

Figure 3 - *Wind Bracing*

The bridge is supported by pinned and rocker bearings which rest on reinforced concrete multi-column bents. The deck has an asphalt overlay and stay-in-place-forms. Unsymmetric, 12 in. deep sidewalks were constructed along either edge of the roadway and the railing is of a relatively light and open design.

Due to concerns related to capacity, in 1997, steel retrofit plates were bolted to the bottom flange of the girders on Spans 2 and 3 at the first bottom flange transitions. Since these plates were installed without shoring, they are only active in resisting live load effects (i.e., dead load and super-imposed dead load effects were locked into the original girders and the composite section, respectively).

Past Load Rating Analysis

Recently, the New Jersey Turnpike requested that HNTB perform a conventional load rating analysis of the MP 28.9 Bridge. This analysis was detailed in a report that was provided to the Drexel team for review.

The analysis conducted by HNTB was carried out using a Virtis XML file that was previously developed by TransSystems. The primary modification made to this file by HNTB was related to the effective length of the retrofit plates applied along the bottom flange. The original file assumed the plates were active over their entire length and did not properly account for the development length associated with the bolted connection.

Using this representation of the bridge, the demands were estimated as follows: (a) the dead load effects were computed assuming no composite action and ignoring the retrofit plates, (b) the superimposed dead load effects were computed assuming full composite action and ignoring the retrofit plates, and (c) the live effects were computed assuming full composite action and considering the retrofit plates over their effective length.

Load ratings were calculated using both the Allowable Stress Rating (ASR) approach and the Load and Resistance Factor Rating (LRFR) approach. Based on these analyses it was determined that the fascia

girder of Span 2 (denoted Girder 6) was the controlling member. Based on the ASR approach, it was found that the controlling member is overstressed and unable to withstand the dead load stresses at both the Inventory and Operating levels. Based on the LRFR approach, it was found that the controlling member had rating factors less than 1.0 for all legal loads, with the controlling case being the Service II Limit State.

Since traffic demand on this structure has decreased significantly due to the decommissioning of the Beasley's Point Bridge, it was concluded that the bridge could remain in service in the near-term, but should be posted at 20 tons. In addition, it was recommended that construction vehicles associated with the replacement of the Great Egg Harbor Bridge (which is adjacent to the MP28.9 Bridge) not be permitted to use the bridge, and that the bridge be considered for replacement.

Site Visit

A site visit was conducted on Tuesday, December 20, 2011 to assess the condition of the structure as well as to evaluate the level of access in preparation for potential experimental testing (Figure 4). During the visit it was noted that the superstructure appeared to be in good condition with some minor surface rust and paint peeling on the girders. Some of the diaphragms did appear to exhibit a larger level of corrosion, though this was difficult to determine when viewing from ground level.

The majority of the bearings were clean and free of debris with the exception of a few locations where water was leaking through the joints or at exterior girder locations. The piers also appeared to be in good condition, with only very local and apparently superficial cracking in some portions of the pier cap that supported Spans 2 and 3. The deck and sidewalks appeared to be in fair condition, with some minor cracking and spalling in a few locations.

Overall the bridge appears to be performing well; there were no obvious signs of structural distress and all observed deterioration was consistent with a well-performing bridge after 50 years of service.

a. Bearing deterioration *b. Surface rust/paint peeling* *c. Retrofit plate*

***Figure 4** – Condition of structure*

During the site visit traffic demand was observed to be quite low. This is attributed to two primary reasons. First, the site visit occurred in December when traffic demand in the entire region is depressed (as summer recreational activities account for the majority of the economic activity in the region). Second, the bridge previously served to connect travelers to the Beasley's Point Bridge, which has now

been removed from service. Of the three lanes on the MP 28.9 Bridge, two of them had primarily carried traffic to and from this bridge. At the current time, the primary use of this bridge is for local traffic traveling westbound and entering the southbound lanes of the Garden State Parkway. The only way for traffic to enter the eastbound lane of the bridge is to travel through the parking lot of the New Jersey Turnpike facility adjacent to the toll plaza.

Conventional Load Rating Analysis

To better understand the apparent load-carrying capacity issues associated with the MP 28.9 Bridge, a conventional load rating analysis was carried out for all interior girders and the controlling girder (G6) within Span 2 (which HNTB found to be the controlling span) using the LRFR method. Given the numerous cross-sectional transitions in each girder (Figure 5), load ratings were computed at the end of each transition (e.g. the portion of the transition closest to mid-span) to identify both the controlling girder and the controlling section of the girder.

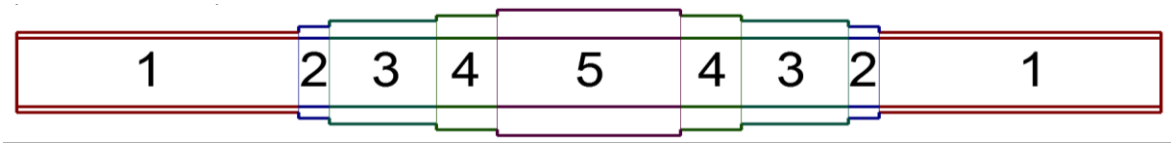

Figure 5 - *Transition section designations used throughout report*

To determine the dead load effects, a tributary-area approach was used to distribute the weight of the deck and sidewalks to the original girder cross-sections (i.e., not including the retrofit plates). The superimposed dead load effects (e.g., the asphalt overlay and railing) were also distributed based on tributary area, but were assumed to be resisted by the long-term composite girder section. Finally, the live load effects were distributed using the AASHTO distribution factors and were assumed to be resisted by the short-term composite section. These effects were computed both including and ignoring the retrofit plate.

A summary of the rating factors for the Strength I and Service II Limit States are provided in Tables 1 and 2, respectively.

Table 1 - *Rating Factors for Interior Girders*

Interior Girders	Strength I Limit State		Service II Limit State	
	Inventory	Operating	Inventory	Operating
Moment RF	*0.78*	*1.00*	*0.50*	*0.65*
Shear RF	*1.35*	*1.75*	-	-

Table 2 - *Rating Factors for Exterior Girder (G6)*

Exterior Girder (G6)	Strength I Limit State		Service II Limit State	
	Inventory	Operating	Inventory	Operating
Moment RF	*0.13*	*0.23*	*0.00*	*0.00*
Shear RF	*0.97*	*1.26*	-	-

Figures 6 and 7 show the variation of demands and capacities (for the Strength I Limit State) along the length of the interior girders and exterior girder (G6), respectively. It is important to recognize that these plots do not convey rating factors, but rather overall safety factors (factored capacity divided by factored demand), but they are informative nonetheless. The interior girders rate for the operating level without considering the retrofit plates and rate for both the operating and inventory levels if the plate is included (Figure 6). In contrast, the controlling exterior girder (G6) does not rate at the first and second transition for either level even when the retrofit plates are considered.

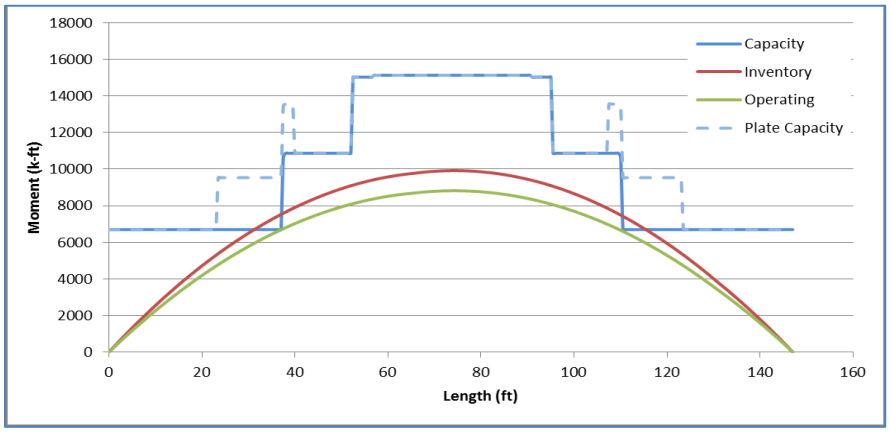

***Figure 6** - Moment capacity and demand for interior girders*

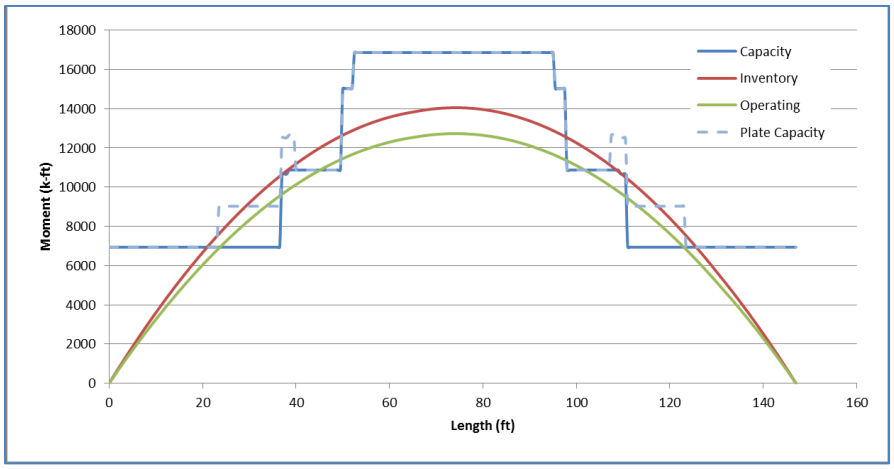

***Figure 7** - Moment demand and capacity for exterior girder (G6)*

A-Priori Modeling and Refined Load Rating Analysis

Given the relatively low load ratings, it is important to identify whether the conventional load rating procedures are reasonably accurate for the MP 28.9 Bridge or if they are excessively conservative. Towards that end, it was decided to develop an element-level FE model to compute the dead load, superimposed dead load, and live load effects. In this approach, the significant assumptions associated with the live load distribution between girders and the effects of skew can be replaced by a mechanistic

model that is a more accurate representation of the MP 28.9 Bridge. The following sections discuss the development of the model, the error screening of the model, and the use of the model to develop refined load ratings.

Model Development

The model resolution selected for the MP 28.9 Bridge is commonly termed “element-level” and is the most common class of FE models employed for constructed systems. This type of model employs both one-dimensional (plane or space frame elements) and two-dimensional elements (e.g. plate or shell elements) to model girders/diaphragms and deck, respectively (Figures 8 and 9). In an effort to remain consistent with the three dimensional geometry of the structure, various link elements (to connect girders to the deck) and constraints (to simulate boundaries) were also employed. Given the many transitions within the girders of the MP 28.9 Bridge, a fairly dense mesh of 6 in. was required to allow the model to properly replicate the geometry.

To account for the different stages of construction, this base model was analyzed using different continuity conditions. For example, to estimate the dead load effects the model was analyzed with hinges included on either side of the link elements that connected the girders and the deck, which allowed the model to perform in a non-composite manner. To estimate the effects of superimposed dead load and live load, the links between the girders and deck were assigned rigid properties, which enforce strain compatibility to simulate composite action. Since it is not reliable to depend on the guard rail and asphalt overlay to provide structural stiffness/capacity, these elements were considered only as superimposed dead loads.

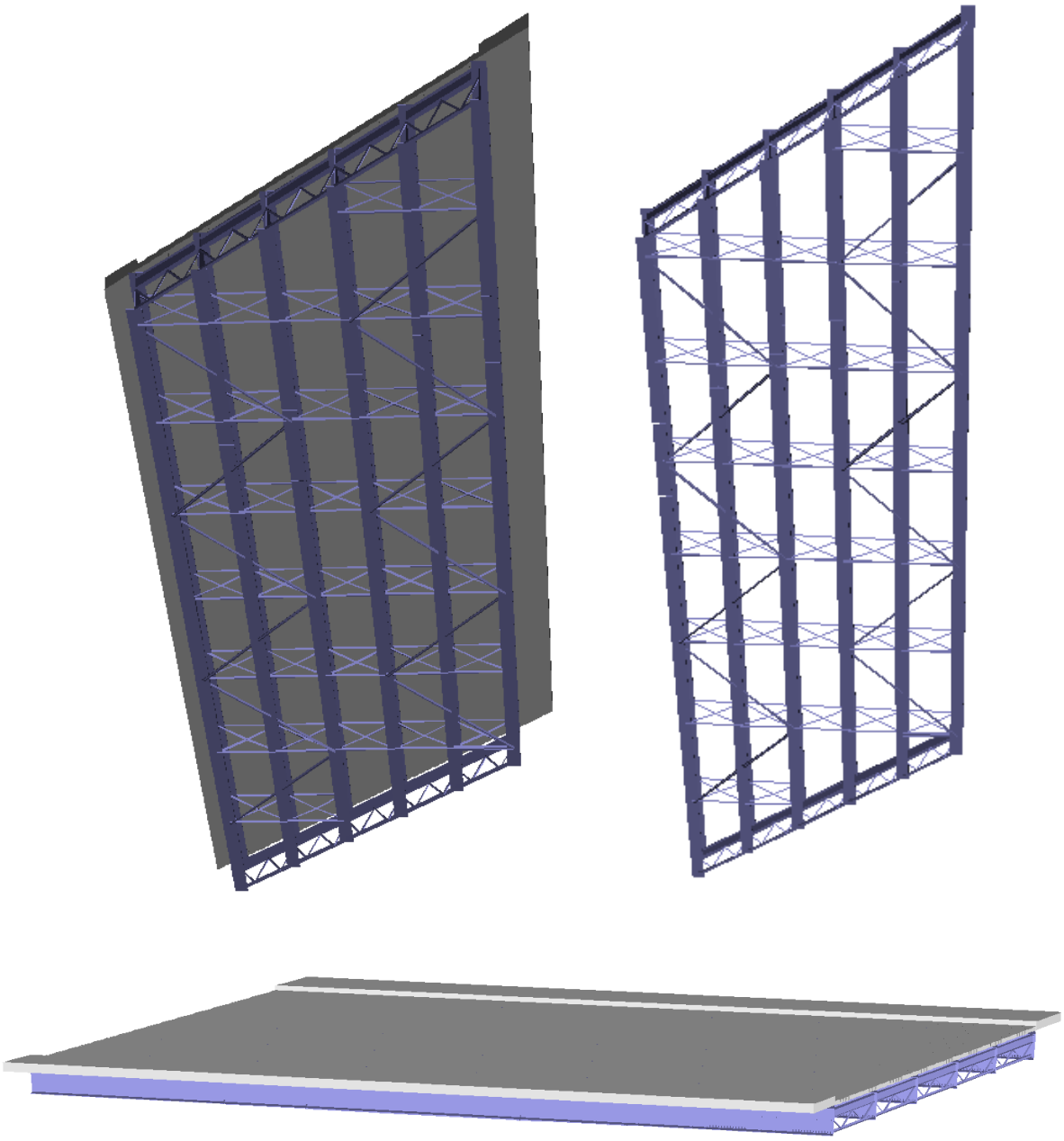

Figure 8 - *FE model of the MP 28.9 Bridge*

To illustrate how the 3D geometry of the bridge was simulated using various elements and links, Figure 10 shows a schematic of both the actual bridge geometry and the FE model at an end of a girder (as an example). The approach used represented all primary members with elements located at their geometric centroid and then connected with link elements (which can be tuned to enforce or relax compatibility). This modeling approach is effectively consistent with the assumptions of cross-sectional behavior that are implicitly included within the conventional load rating procedures.

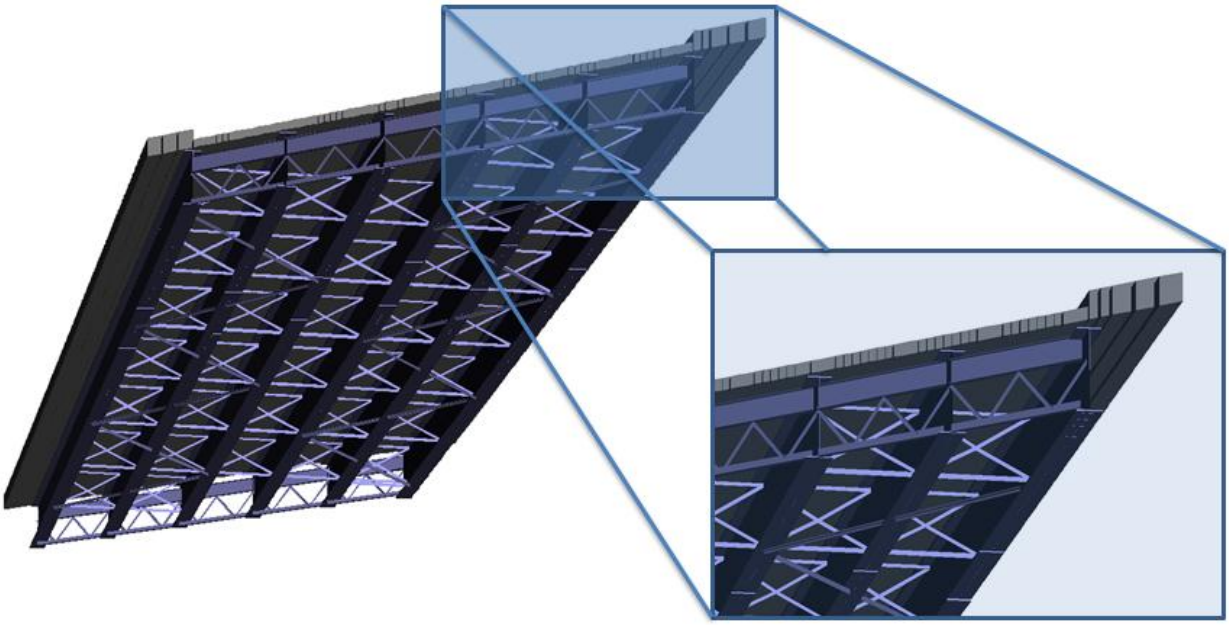

Figure 9 – *Close-up view of model geometry*

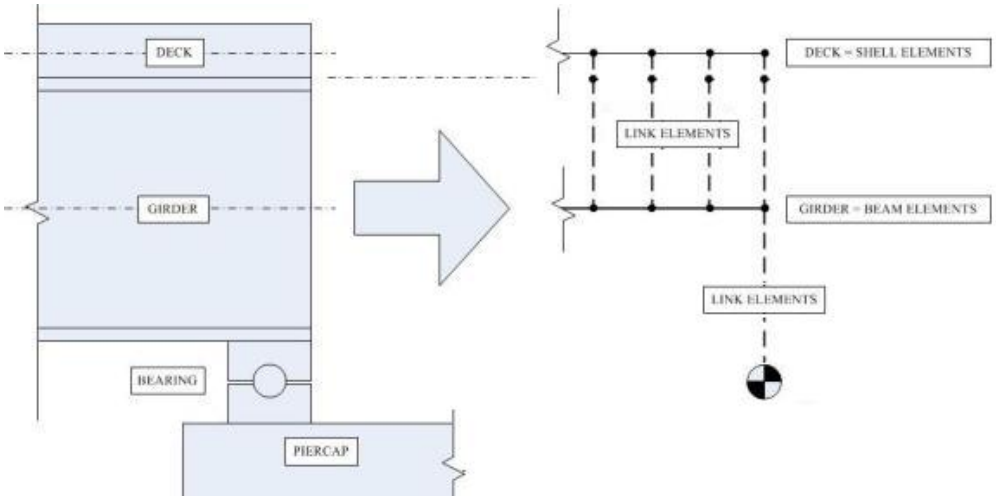

Figure 10 – *Comparison of actual geometry and model geometry*

The steel members were modeled with a modulus of 29,000 ksi and a yield stress of 36 ksi. The concrete deck was assigned a modulus and compressive strength of 3,155 ksi and 3 ksi, respectively, and the deck was modeled as uncracked for two reasons. First, no reflective cracks were observed in the asphalt overlay during the site visit. Second, as AASHTO Comment 4.5.2.2 (AASHTO 2007) points out: “Tests indicate that in the elastic range of structural behavior, cracking of concrete seems to have little effect on the global behavior of bridge structures. This effect can, therefore, be safely neglected by modeling the concrete as uncracked for the purposes of structural analysis (King et al. 1975)”.

The continuity conditions for the diaphragms were modeled as fixed for the load rating analysis, but pinned conditions were analyzed as well and produced negligible differences. The *Construction Sequence* noted in the As-Built plans on sheet 47/97 states that the diaphragms are to be fastened with erection bolts prior to the concrete deck being poured. The bolts were to be loosened and retightened after the deck pour. It is unlikely that this sequence would drastically redistribute dead load stresses amongst the girders for several reasons. First, by the time the bolts were loosened and re-tightened the deck would have stiffened and would have maintained the dead load distribution of the girders. Second, the bolts likely were placed into bearing due to the significant deformations that are caused during the pouring of the deck. Third, the loosening and re-tightening of the diaphragms bolts would have likely been done sequentially (as opposed to all at once).

Error Screening

Once the model was constructed, a rigorous error screening procedure was carried out to ensure the intended mechanisms, continuity conditions, and boundary conditions, etc. were properly simulated. This included (a) identification and elimination of duplicate elements, nodes, links, etc., (b) the use of equilibrium to check global reactions and local actions, (c) examination of global deflected shapes to ensure compatibility was satisfied, (d) comparisons with simplified analysis approaches to estimate actions and displacements, and (e) examination of global mode shapes for physical consistency.

Results and Model-based Load Rating

Once the model was error screened it was employed to estimate the dead load, superimposed dead load and live load effects for the Service II Limit State (which controlled using the conventional load rating approach). The analysis was carried out using an HL 93 live load model and considering moving truck loads in each lane, variable axle spacing, and multiple presence. For each location considered (associated with the ends of the transitions as defined previously) the maximum total fiber stresses were extracted from the model to compute the load rating factors. The total fiber stresses include the stresses caused by in-plane bending, axial forces, torsion, and out-of-plane bending. Figure 11 shows an example of typical axial force and bending moment diagrams along with a plot of the total fiber stress distribution within a cross-section at a girder transition.

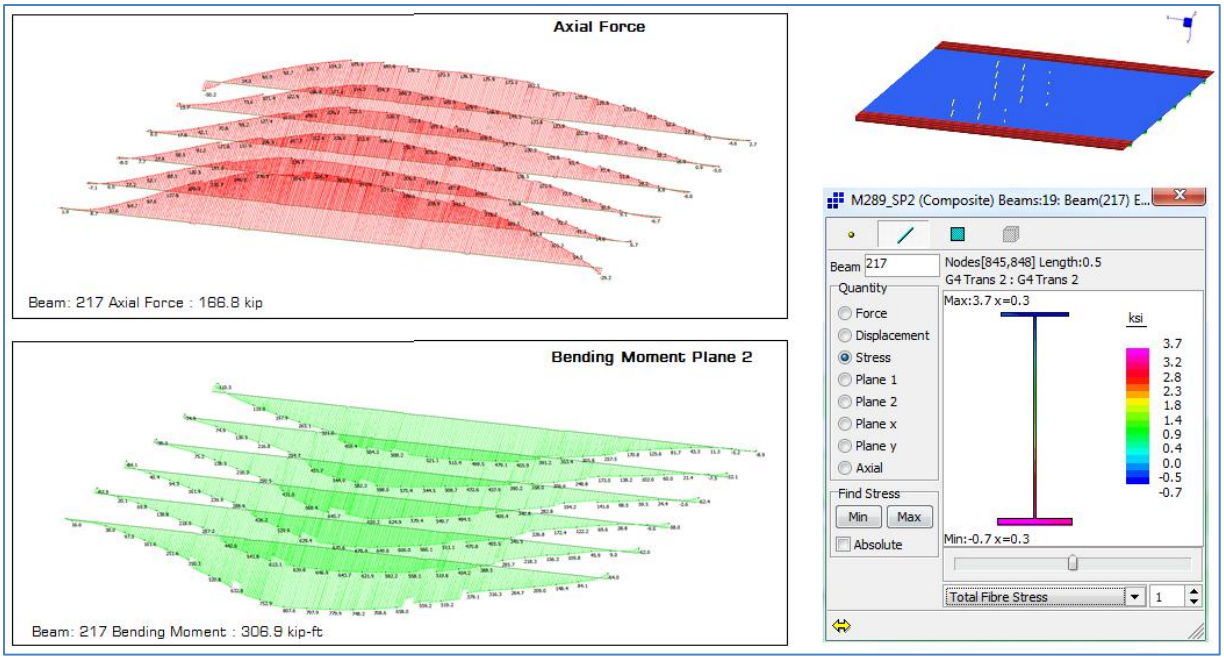

***Figure 11** – Sample results for the governing live load at the first transition of G1*

For each transition, the maximum dead load, superimposed dead load, and live load stresses (considering all truck positions) were extracted to compute the rating factors. To save computational time, the trucks were only run in one direction (e.g., east to west), and thus the ratings of the various transition sections were assigned the lower rating of either the east or west half of the span.

Table 3 shows an example (Girder 2) of the maximum computed stresses for each transition. Table 4 and Table 5 present the refined rating factors computed for each transition of each girder. Considering the effects from dead load, superimposed dead load, and live load computed from the FE model, each girder has rating factors greater than 1.0 for both inventory and operating levels. These results are not uncommon, as many bridges subjected to refined analysis show a decrease in computed demands (compared to conventional load rating procedures) and thus an increase in the related rating factors. In addition, rating factors were calculated for the diaphragm members, and lowest values for each element are shown in Table 6.

***Table 3** – Computed stressed from the FE model for Girder 2*

Girder 2	DC1	DC2 & DW	Sum DL	LL+IM	Inventory	Operating
Transition No.	Stress (ksi)	Stress (ksi)	Stress (ksi)	Stress (ksi)	RF	RF
1	23	1.4	**24.4**	**5.8**	**1.30**	**1.69**
2	13.5	0.8	**14.3**	**3.5**	**4.44**	**5.77**
3	16.5	1.2	**17.7**	**4.8**	**2.66**	**3.46**
4	12	0.9	**12.9**	**3.6**	**4.56**	**5.93**
5	12	0.9	**12.9**	**3.3**	**5.01**	**6.51**
				RF	**1.30**	**1.69**

***Table 4** – Computed Inventory rating factors for each transition of each girder for Service II Limit State*

Transition No.	Girder 1	Girder 2	Girder 3	Girder 4	Girder 5	Girder 6
1	1.29	1.30	1.34	1.55	1.44	1.59
2	4.71	4.44	4.22	4.53	5.15	5.21
3	2.91	2.66	2.94	3.09	3.47	3.95
4	4.97	4.56	5.21	5.89	6.86	8.87
5	4.62	5.01	5.90	6.74	7.02	7.58
RF	***1.29***	***1.30***	***1.34***	***1.55***	***1.44***	***1.59***

***Table 5** – Computed Operating rating factors for each transition of each girder for Service II Limit State*

Transition No.	Girder 1	Girder 2	Girder 3	Girder 4	Girder 5	Girder 6
1	1.68	1.69	1.74	2.02	1.88	2.07
2	6.12	5.77	5.49	5.89	6.69	6.77
3	3.78	3.46	3.82	4.02	4.51	5.13
4	6.46	5.93	6.77	7.66	8.92	11.53
5	6.01	6.51	7.67	8.76	9.13	9.86
RF	***1.68***	***1.69***	***1.74***	***2.02***	***1.88***	***2.07***

***Table 6** – Lowest operating rating factors for each diaphragm member*

Diaphragm Member	Lowest Rating Factor
L3x3x3/8	***2.92***
L4x4x5/8	***2.99***
18WF50	***2.40***
ST6WF	***2.65***

Comparison of Conventional and Model-based Load Rating Analysis

To understand the causes for the differences between the conventional and model-based load rating factors, it is necessary to compare them both from a demand (e.g., dead load, live load) and a spatial perspective. Table 6 shows the total dead load and live stresses computed from both the conventional and model-based load rating for Girder 2, which was the controlling interior girder. Table 7 and 8 show the inventory and operating load rating factors computed from both the conventional and model-based load rating analysis.

Table 7 – Comparison of computed stresses

Girder 2	Model Based	Conventional	Model Based	Conventional
	Total DL	Total Dl	LL+IM	LL+IM
Transition No.	Stress (ksi)	Stress (ksi)	Stress (ksi)	Stress (ksi)
1	24.40	24.56	5.81	14.88
2	14.30	14.47	3.45	8.79
3	17.70	16.20	4.77	10.30
4	12.90	11.75	3.59	7.42
5	12.90	12.17	3.27	7.77

Table 8 – Comparison of Inventory Rating Factors

	Model Based Load Rating						Conventional	
Transition No.	Exterior	Interior Girder				Exterior	Exterior (Girder 6)	Interior
	Girder 1	Girder 2	Girder 3	Girder 4	Girder 5	Girder 6		
1	1.29	1.30	1.34	1.55	1.44	1.59	0.0 (-0.11)	0.50
2	4.71	4.44	4.22	4.53	5.15	5.21	0.82	1.73
3	2.91	2.66	2.94	3.09	3.47	3.95	0.56	1.34
4	4.97	4.56	5.21	5.89	6.86	8.87	0.97	2.33
5	4.62	5.01	5.90	6.74	7.02	7.58	1.55	2.18
RF	*1.29*	*1.30*	*1.34*	*1.55*	*1.44*	*1.59*	*0.0 (-0.11)*	*0.50*

Table 9 – Comparison of Operating Rating Factors

	Model Based Load Rating						Conventional	
Transition No.	Exterior	Interior Girder				Exterior	Exterior (Girder 6)	Interior
	Girder 1	Girder 2	Girder 3	Girder 4	Girder 5	Girder 6		
1	1.68	1.69	1.74	2.02	1.88	2.07	0.0 (-0.15)	0.65
2	6.12	5.77	5.49	5.89	6.69	6.77	1.06	2.25
3	3.78	3.46	3.82	4.02	4.51	5.13	0.72	1.75
4	6.46	5.93	6.77	7.66	8.92	11.53	1.27	3.03
5	6.01	6.51	7.67	8.76	9.13	9.86	2.02	2.83
RF	*1.68*	*1.69*	*1.74*	*2.02*	*1.88*	*2.07*	*0.0 (-0.15)*	*0.65*

The computation of dead load effects was essentially the same between the conventional and the model-based load rating for the interior girders. This is not uncommon as the use of tributary area to distribute uniform dead loads to interior girders (as employed in the conventional analysis) is a fairly accurate means of simplification. In addition, since the deck is not active in the model used to compute dead load effects (i.e., the model is non-composite), the girders behave somewhat independently and thus approximate the single-line girder model.

In contrast, the exterior girder dead load stresses in the model were slightly lower than the conventional load rating analysis calculations. This results from the conventional load rating analysis not considering the sharing of load through diaphragms and the effect of the skew (which are different for exterior and interior girders). Independently these factors may not cause a difference but together they influence the load distribution across the girders and supports. Especially in cases where a diaphragm connects one girder at approximately quarter-span to a section close to a support on the adjacent girder; essentially shedding the load directly into the support causing the exterior girder to have reduced dead load stress.

In the case of the MP 28.9 Bridge the differences between the computed live load effects indicates that the distribution factors (together with the inability to properly address the fairly large skew) have rendered the conventional load rating approach excessively conservative. The live load effects vary significantly between the conventional and model-based load rating analysis, with the FE model computing less than half the live load effects. This difference between the comparison of dead load and live load effects results from both the complexity of loading and structural response associated with live load. The live load model is composed of several combinations of single and multiple trucks that traverse the structure and apply loads in a fairly local region. This type of loading activates the transverse distribution mechanisms of the bridges far more than a uniformly applied dead load, and thus a tributary area distribution approach is inappropriate.

As a result, the use of distribution factors is required to assign truck weights to various girders in the conventional load rating approach. Given the large number of configurations these distribution factors cover, they necessarily tend to be highly conservative (especially as their primary value is in supporting new design). According to this analysis, the MP 28.9 Bridge rates for both operating and inventory levels for the Strength I and Service II Limit States. While, strictly speaking, the model-based load ratings could be accepted as is (as per AASHTO); to ensure the validity of the model, it was compared with response measurements acquired directly from the bridge.

Test Program Design

A rapid testing program to capture key response metrics directly from the bridge was designed in order to validate the model used in the refined load rating analysis. Given the similar nature of Spans 2 and 3 (which control the rating), the testing program focused on Span 2 as the required traffic control for this span was less disruptive.

The various response metrics captured included relative measures (e.g., live load distribution factors, degree of composite action), absolute measures (e.g., vertical displacement and strain profiles), and operating responses (e.g., impact factors, short-term strain and displacement histograms). The testing

program also aimed to measure the degree to which the retrofit plates were active in resisting live load actions. To capture such response metrics, two testing approaches were employed:

Phase 1 - The monitoring of responses under ambient traffic excitation

Phase 2 - Crawl-speed tests and static testing of the span using two trucks loaded to approximately 65 kips each

To ensure the efficient and rapid execution of these tests on the MP 28.9 Bridge a single, integrated instrumentation plan was developed and is shown schematically in Figure 12. Of particular interest during the design was to locate the instrumentation in such a way that all critical responses could be captured while not putting undue burden on the traffic control and access issues. Instrumentation for Phases 1 and 2 included 22 high-speed strain gages, and 8 displacement gages.

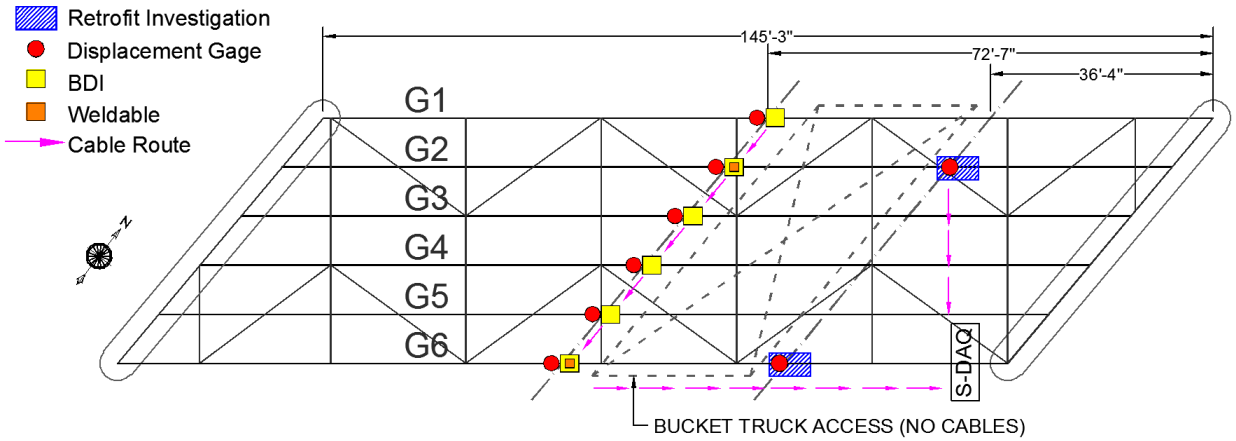

Figure 12 - Sensor installation layout plan

Test Execution

The test was carried out on March 6, 2012. Installation of gages began at 8:30 am and lasted until 10:00 am. Due to limited underside access, sensors were installed only on the east half of Span 2 as shown in the instrumentation plan (Figure 12). Displacement sensors and pairs of removable strain gages were installed on the bottom flange of each girder at mid-span (Figure 13). Weldable strain gages were attached to Girders 2 and 6 at four locations on the cross-section at the retrofit plate and on the web at mid-span (Figure 14). The data acquisition equipment was located south of the pier between Spans 2 and 3.

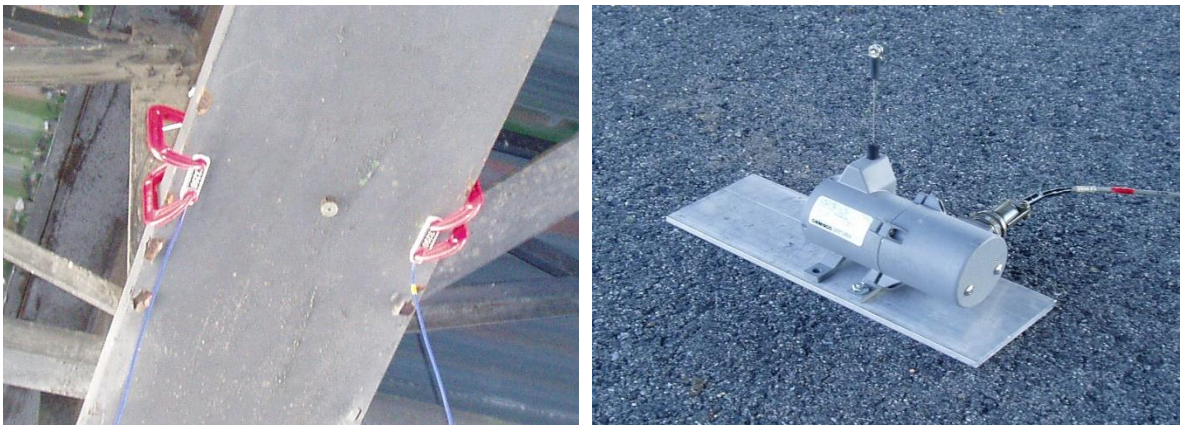

Figure 13 - Midspan strain and displacement sensors

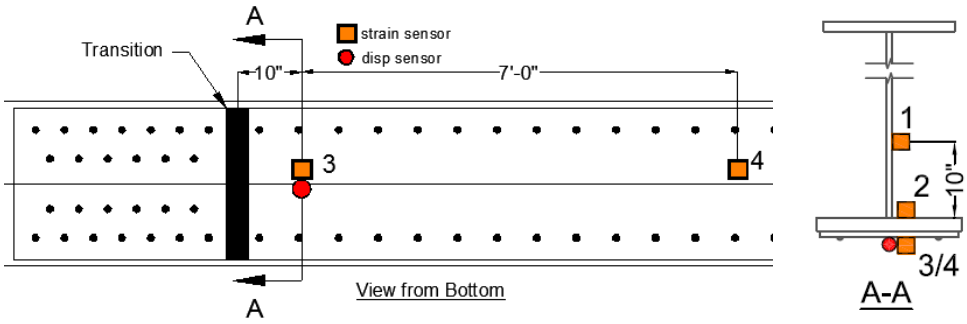

Figure 14 - Weldable strain sensors at retrofit location

To compensate for the lack of truck traffic on the MP28.9 Bridge, two trucks were run across the bridge continuously to ensure that meaningful responses were captured during Phase 1, which lasted for approximately two hours. Phase 2 consisted of both crawl-speed and static testing of the span using two trucks loaded to approximately 65 kips (Figure 15), and lasted approximately three hours. All equipment and cabling was removed from the bridge by 5:30 pm.

Figure 15 - *Static truck load positioning at mid-span*

Data Acquisition

National Instruments equipment was chosen for the data acquisition system for this test due to its functionality and versatility. For this test, a 24-bit synchronous cRIO data acquisition system was used to sample data from 8 displacement sensors (potentiometers), 12 BDI strain sensors, and 10 electrical-resistance weldable strain sensors. Military connectors were attached to the outside of the data acquisition box, and wired directly to the data acquisition cards for easy hook-up. During all phases data was sampled at 100 Hz.

Real-time data interpretation and quality assurance was accomplished through visualization modules developed using Lab-View. The first panel, shown in Figure 16, was developed for the monitoring phase under normal traffic demand and provides strain and displacement measurements as a function of time for the gages installed on the bottom flange of each girder at mid-span. Since each girder had a strain sensor on either flange, the two individual strain measurements, along with the average, were plotted in order to make sure each sensor was reading properly. This also provided insight into the level of out-of-plane bending. To convey the spatial location of the sensors, the panel has an instrumentation plan in the lower left hand corner that lights up the sensors that are being shown in the time history plots.

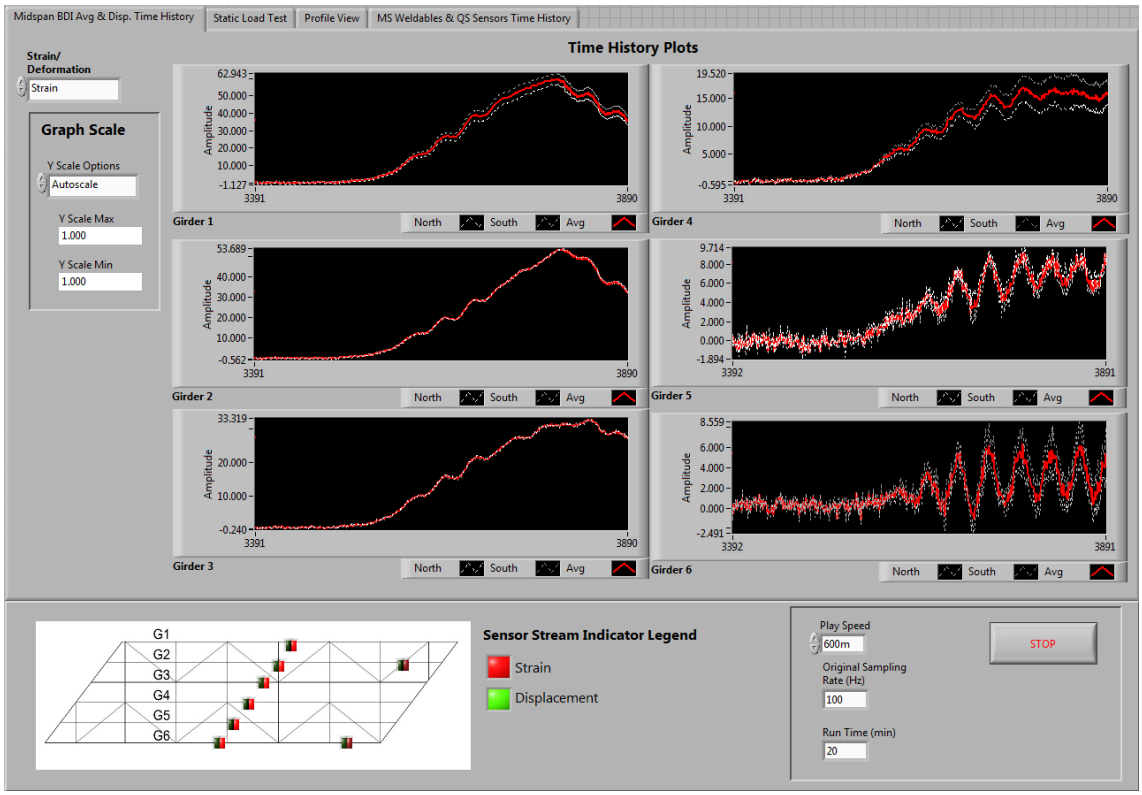

***Figure 16** - On-site data visualization software - monitoring of mid-span strains*

The next two panels were developed for the second phase. Using the measurements from the strain sensors installed on Girders 2 and 6, the neutral axis location is plotted at both the mid-span and the retrofit location (Figure 17). The level of composite action can be evaluated by comparing these values with the calculated neutral axis locations for the conventional load rating analysis. Mid-span displacement and strain profiles are also plotted spatially to allow on-site data interpretation and comparison with expected responses from the model (Figure 18). Finally an additional panel was developed to show the raw data from all of the weldable strain sensors for quality control, quality assurance.

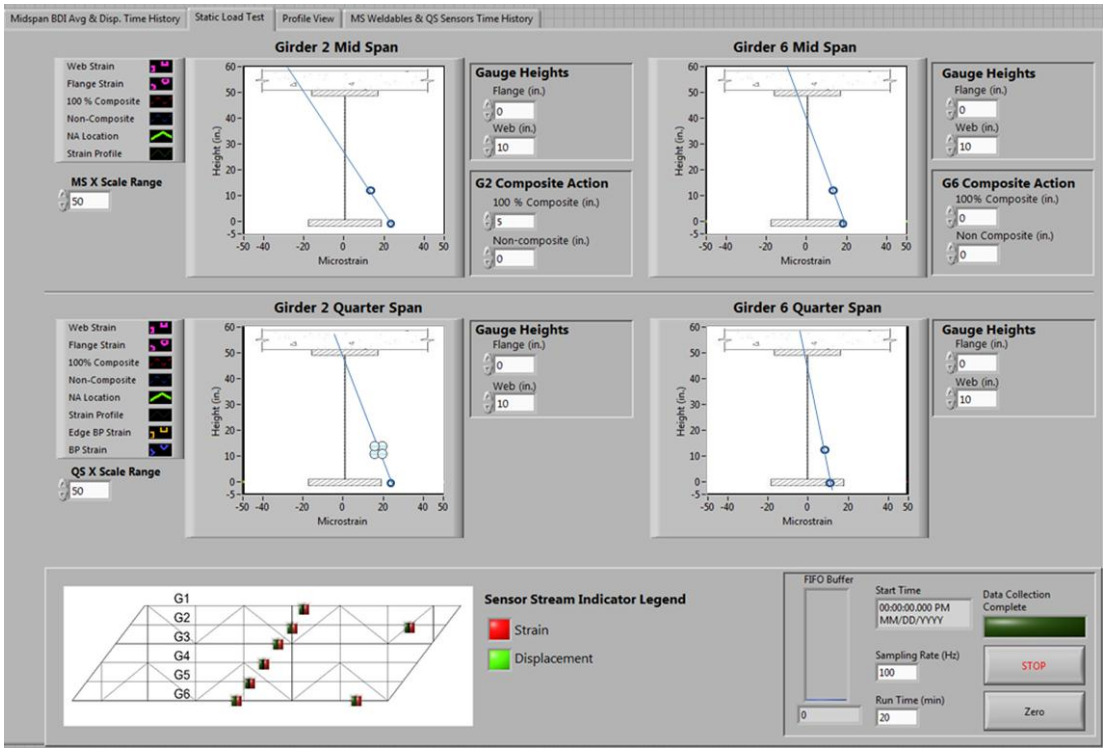

Figure 17 - *On-site data visualization - neutral axis plots*

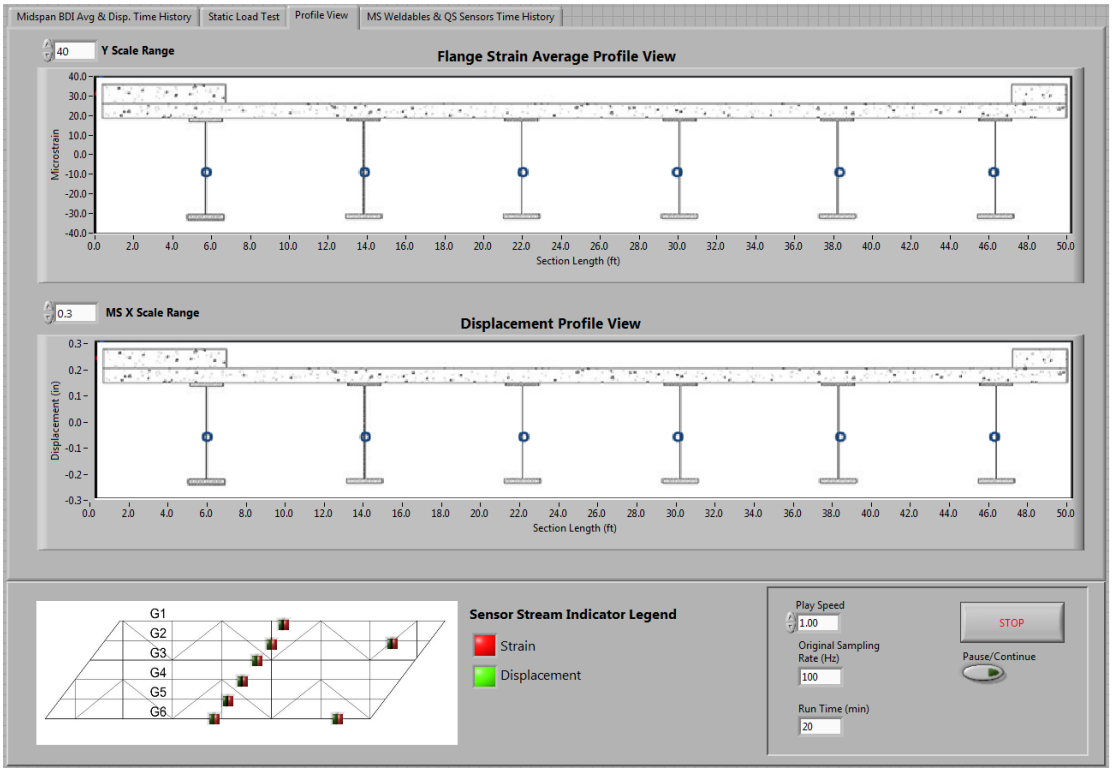

Figure 18 - *On-site data visualization software - strain and displacement profiles*

Data Processing and Visualization

An automated data processing program was developed in order to quickly process each data set and extract pertinent information about the performance of the bridge. Sensors are grouped into families based on the type of response, and sensor location. The raw time histories of these families are plotted to check for any blatant anomalies. The data was subjected to a low-pass filter to reduce any effects from high frequency noise. If there was appreciable drift present in the response for any sensor, the trend was removed and any offsets were subtracted. For comparison purposes, plots of both raw and cleaned data streams are shown in (Figure 19).

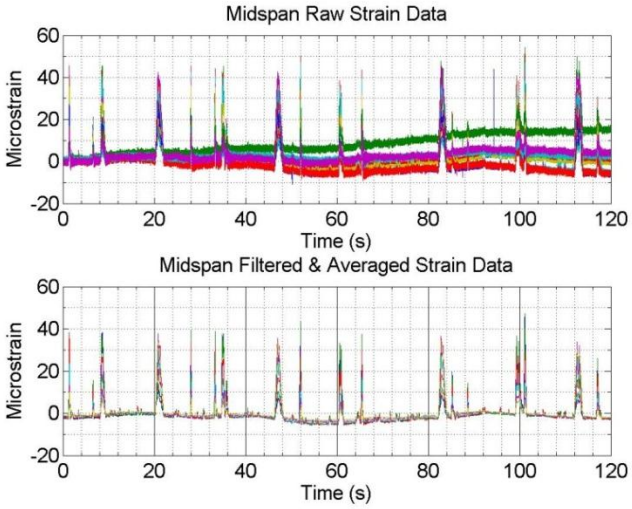

Figure 19 - *Example of raw and processed mid-span strain data*

Data Interpretation

Once the data was processed, many relationships were examined to better understand the actual behavior of the bridge. Considering that operational monitoring of a bridge for determining distribution factors, strain/displacement profiles, and experimental load ratings is still being developed, the static load test along with the crawl speed tests were crucial to verify all findings extracted from the monitoring data. Data interpretation for both phases is described in the following sections.

Phase 1 – Monitoring Results

The first step of the automated feature extraction program was to recognize truck events and distinguish which lane the vehicle was positioned in. The “cleaned” data was then plotted with markers designating these truck events for visual verification (Figure 20).

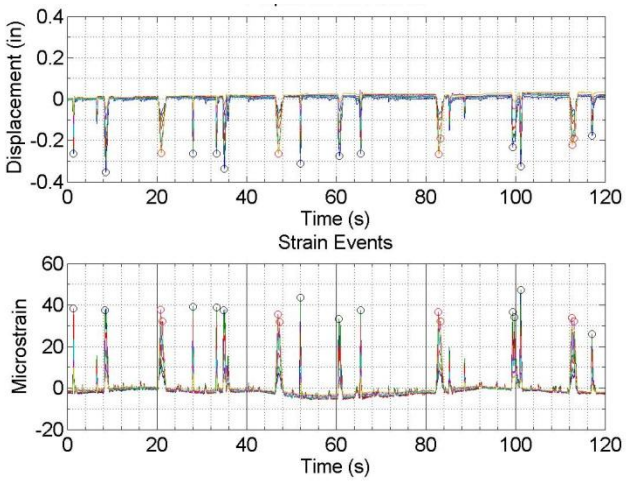

Figure 20 - *Distinguish peak truck events*

For each truck event, operational distribution factors were calculated. Box plots were developed showing the distribution factors based on strains and displacements as well as lane position (Figure 21). The red center line signifies the median distribution factor for that girder for all the truck events. The lower and upper limits of the box signify the 25th and 75th percentile, and the lower and upper bars indicate the lowest and highest experimentally observed distribution factors. Using conventional load rating procedures, the exterior girders have a distribution factor of 0.67 and the interior girders have a distribution factor of 0.56. Experimentally, the highest distribution factor measured was 0.33.

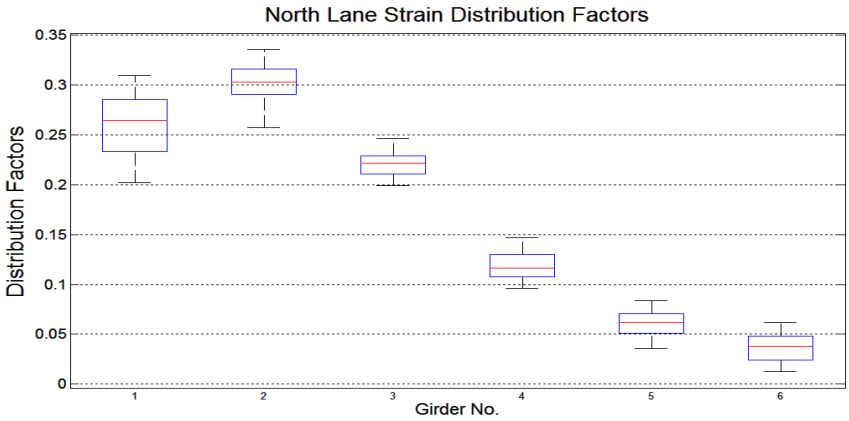

Figure 21 - *Distribution Factors for trucks in north lane and south lane*

The composite and non-composite neutral axis locations were calculated previously for the conventional load rating analysis (assuming a standard effective width of the deck). For full composite action, the neutral axis should be located approximately 52 in. above the bottom flange at quarter-span. The results for Girders 2 and 6 indicate that the bridge is in fact fully composite with the quarter-span neutral axis locations being 69 in. and 62 in. respectively (Figure 22). The reasons that the measured neutral axes were higher than the fully-composite calculated ones include (1) the use of a conservative estimate for effective width, (2) the use of a conservative estimate of the elastic modulus of concrete, and (3) the

fact that the calculations did not consider the stiffness of the overlay. Additionally it should be mentioned that this interpretation approach depends on extrapolating the strain profile to its zero crossing and it therefore is sensitive to noise and small bias errors.

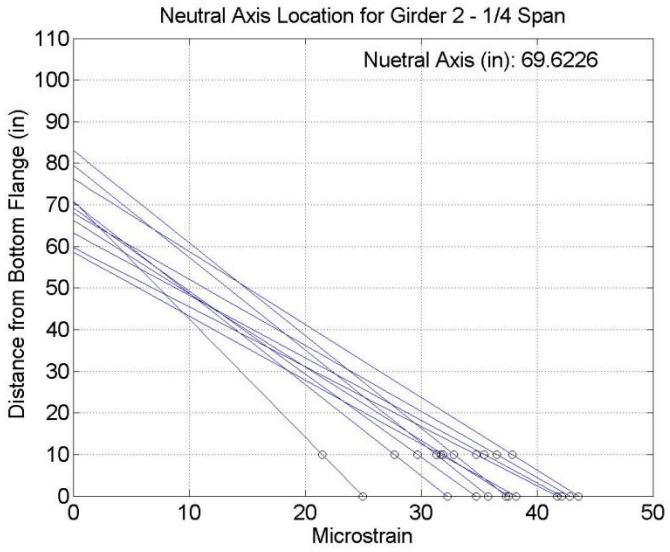

Figure 22 - *1/4 span neutral axis locations for Girder 2*

The strains measured on the retrofit plates were approximately equal to the strains measured on the parent girder indicating that the retrofit plates were actively resisting live load. Figure 23 below shows the mid-span strain (located at 0 ft. on the plot), the strain value from the sensor installed on the bottom flange 10 in. from the first transition (located at 35 ft. on the plot), the sensor installed on the underside of the retrofit plate 10 in. from the first transition (also located at 35 ft. on the plot) and the additional sensor located on the retrofit plate 7 ft. from the first transition (located at 42 ft. on the plot). The two sensors located on the bottom flange and the underside of the retrofit fit plate (located at 35 ft. on the plot), have a small difference in magnitude showing that the retrofit plate is indeed active. The additional sensor located further down the retrofit plate (located at 42 ft.) shows the retrofit plate is also developed over that length.

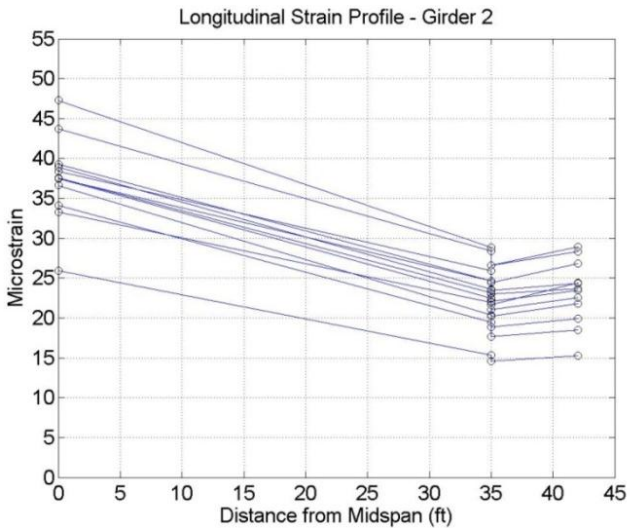

Figure 23 - *Longitudinal strain profiles for Girder 2*

Experimental impact factors were determined by comparing the measured time history responses with the extracted static responses. The extracted static response was found by filtering out the low frequency dynamic oscillation of the bridge from the raw data and comparing the maximum response in the raw time history with the maximum response in the extracted static response. The maximum measured impact factor was 1.15.

Phase 2 – Static and Crawl-Speed Truck Load Test Results

The static truck load test consisted of four different vehicle configurations within the traffic control area. The three single truck positions used were in the south lane at ¼ -span, mid-span, and at ¾ -span. The fourth configuration was two trucks located in the south and middle lanes at mid-span. The maximum mid-span responses for both strain and displacement occurred during the two truck loading configuration (Figures 24 and 25). Both the maximum strain and displacement occurred on Girder 5 with magnitudes of 43 με and -0.31 in., respectively. In all cases the bridge returned to its original position following the removal of the load, which indicates all responses measured were elastic in nature.

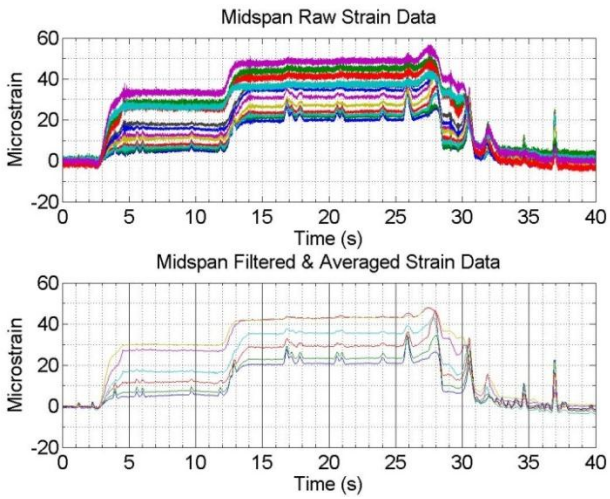

Figure 24 – *Static Truck Load Test – 2 trucks – mid-span raw & processed strains*

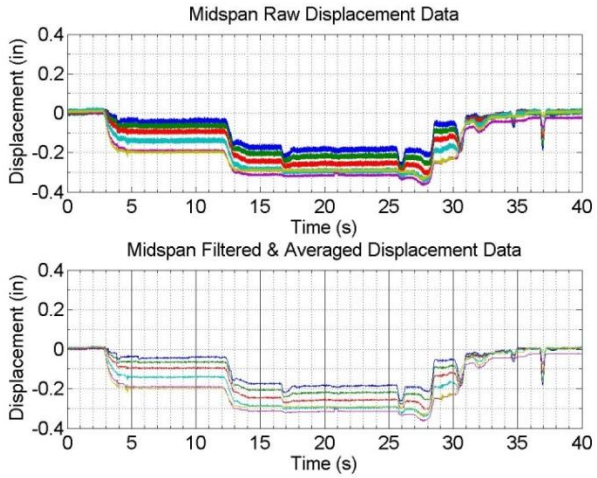

Figure 25 – *Static Truck Load Test – 2 trucks – mid-span raw & processed displacements*

Model-Experiment Correlation

Immediately after completion of the test, the model was updated to include the axle loads used for the four configurations of the static truck load phase. Displacement and strain responses were then extracted from the model at the sensor locations from the test. Comparisons between the model results and the true measurements were carried out. This comparison revealed that all of the measured displacements and strains were smaller than those predicted by the model.

Typically there was a 5 to 15% decrease in displacement as compared to the model predictions. The analytical (i.e., model) and measured displacements for the load case with a single truck in the South Lane at mid-span are plotted in Figure 26 (for reference, Girder 6 is located on the west side of the bridge and Girder 1 is located on the east side of the bridge). All of the measured strains were 20 to

40% lower than the predicted values from the model. The analytical and measured strains from the same load case are plotted in Figure 27. For all static truck load cases, the model had maximum distribution factors ranging between 0.23 and 0.33 (which were consistent with those measured during Phase 1).

Such discrepancies between an FE model and real test measurements are common. Though the FE model is a good representation of the actual bridge there are many mechanisms that are not represented accurately. For example, while the weights of the barrier and asphalt overlay are included as surface loads, their stiffness contributions are ignored. In addition, the stiffness of the longitudinal stiffeners on the exterior girders has been neglected. Further the support conditions for the superstructure were modeled as idealized pins and rollers, which neglect any partial restraint to longitudinal displacement (and the resulting negative moment) that may occur in reality. These conservative simplifications notwithstanding, overall the FE model appears to represent the observed behavior of the bridge quite well (albeit slightly conservatively).

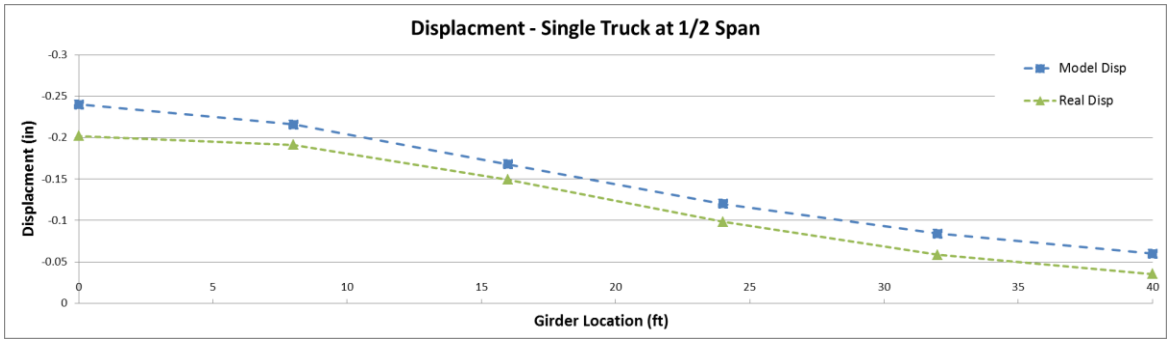

Figure 26 - *Comparison between model and measured displacements*

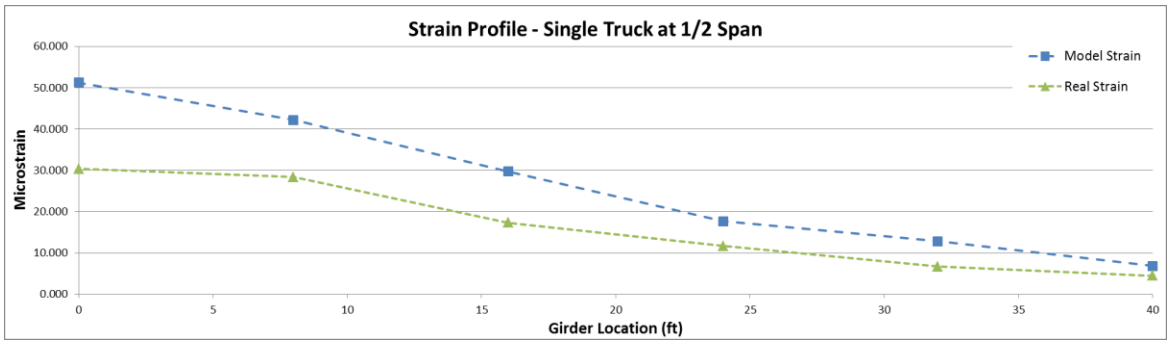

Figure 27 - *Comparison between model and measured strains*

Model-Based Rating Factors for Various Construction Vehicles

Following the validation of the FE model, a series of rating factors were computed for construction vehicles that may be required to use the bridge during the replacement of the nearby Great Egg Harbor Bridge. Table 9 provides the designations, axle weights and axle spacings for each vehicle considered.

Each vehicle was input into the model with a multiple presence factor of 1.2 in order to compare with the conventional load rating calculations completed (only the single lane case was considered for these construction vehicles). The responses from the model were then used to calculate distribution factors and rating factors.

For all five load cases the mid-span distribution factors were consistent, with the highest distribution factor being 0.20 (Table 10). The rating factors were calculated using three impact factors; the code-specified impact factor of 1.33, the maximum experimentally measured impact factor of 1.15, and 1.00 which reflects the impact factor for vehicles crawled across the bridge at 5 mph.

Table 10 – *Overload vehicle dimensions and weights*

C-4-108		
Axle	Weight (kips)	Spacing (ft)
1	27	5.5
2	27	6.5
3	27	5.5
4	27	

C-5-135		
Axle	Weight (kips)	Spacing (ft)
1	27	8
2	27	5.5
3	27	5.5
4	27	5.5
5	27	

OT-3-70		
Axle	Weight (kips)	Spacing (ft)
1	14	17
2	28	4.5
3	28	

OT-4-78		
Axle	Weight (kips)	Spacing (ft)
1	12	15
2	22	4.5
3	22	4.5
4	22	

OT-5-100		
Axle	Weight (kips)	Spacing (ft)
1	12	15
2	22	4.5
3	22	4.5
4	22	4.5
5	22	

Table 11 – *Model-based Distribution Factors for overload vehicles*

Girder	C-4-108	C-5-135	OT-3-70	OT-4-78	OT-5-100
1	0.19	0.19	0.20	0.19	0.19
2	0.17	0.17	0.17	0.17	0.17
3	0.14	0.14	0.15	0.15	0.14
4	0.14	0.15	0.13	0.14	0.15
5	0.17	0.17	0.17	0.17	0.17
6	0.18	0.18	0.17	0.17	0.18

All of the controlling rating factors occurred at the retrofit locations for each load case. The operating rating factors for each vehicle considered are presented in Tables 11 to 15. A conventional load rating was also completed for each vehicle configuration for an interior girder and for the controlling exterior girder (Girder 6). The model-based rating factors were then compared to the conventional analysis to determine whether there is a single scaling factor that could be used to estimate the model-based factors from the conventional ones. It should be noted that scaling factors are not provided for Girder 1, since a conventional load rating was not completed for this girder, and for Girder 6 since the rating factors determined through the conventional load ratings were zero for all five vehicles considered.

As apparent from Tables 11 to 15, all girders had model-based rating factors above 1.0 when considering crawling vehicles (i.e. an impact factor of 1.0). With the exception of Girder 6, all girders had a model-based rating factor above 1.16 when an impact factor of 1.15 was assumed, which is the highest experimentally measured impact factor. Again, with the exception of Girder 6, all girders had a model-based rating factor above 1.01 when an impact factor of 1.33 was assumed. The lowest scaling factor determined was 1.12 and the highest scaling factor was 3.41. Since the scaling factors have a wide range depending on the truck configuration, a simple scaling of conventional load ratings will not be reliable.

***Table 12** - C-4-108 Rating Factors and Scaling Factors*

C-4-108	Conventional	Model			Scaling
	IM = 1.33	*IM = 1.33*	*IM = 1.15*	*IM = 1.00*	*IM = 1.00*
Girder 1	NA	1.01	1.16	1.34	***NA***
Girder 2	0.90	1.03	1.19	1.36	***1.12***
Girder 3	0.90	1.15	1.33	1.53	***1.28***
Girder 4	0.90	1.66	1.92	2.21	***1.52***
Girder 5	0.90	1.04	1.21	1.39	***1.13***
Girder 6	-0.21	0.76	0.88	1.01	***NA***

***Table 13** - C-5-135 Rating Factors and Scaling Factors*

C-5-135	Conventional	Model			Scaling
	IM = 1.33	*IM = 1.33*	*IM = 1.15*	*IM = 1.00*	*IM = 1.00*
Girder 1	NA	1.67	1.93	2.22	***NA***
Girder 2	0.72	1.73	2.00	2.31	***2.36***
Girder 3	0.72	1.92	2.22	2.56	***2.73***
Girder 4	0.72	2.40	2.77	3.19	***3.02***
Girder 5	0.72	1.84	2.13	2.45	***2.44***
Girder 6	-0.17	1.30	1.51	1.73	***NA***

***Table 14** - OT-3-70 Rating Factors and Scaling Factors*

OT-3-70	Conventional	Model			Scaling
	IM = 1.33	*IM = 1.33*	*IM = 1.15*	*IM = 1.00*	*IM = 1.00*
Girder 1	NA	3.23	3.74	4.30	***NA***
Girder 2	1.33	3.21	3.71	4.27	***2.43***
Girder 3	1.33	3.56	4.12	4.74	***2.74***
Girder 4	1.33	5.28	6.10	7.02	***3.41***
Girder 5	1.33	3.26	3.77	4.34	***2.48***
Girder 6	-0.31	2.62	3.03	3.49	***NA***

Table 15 - OT-4-78 Rating Factors and Scaling Factors

OT-4-78	Conventional	Model			Scaling
	IM = 1.33	*IM = 1.33*	*IM = 1.15*	*IM = 1.00*	*IM = 1.00*
Girder 1	NA	3.00	3.47	3.99	***NA***
Girder 2	1.21	2.95	3.42	3.93	***2.43***
Girder 3	1.21	3.30	3.81	4.38	***2.77***
Girder 4	1.21	4.45	5.14	5.92	***3.23***
Girder 5	1.21	3.01	3.49	4.01	***2.48***
Girder 6	-0.28	2.31	2.67	3.07	***NA***

Table 16 - OT-5-100 Rating Factors and Scaling Factors

OT-5-100	Conventional	Model			Scaling
	IM = 1.33	*IM = 1.33*	*IM = 1.15*	*IM = 1.00*	*IM = 1.00*
Girder 1	NA	2.34	2.71	3.12	***NA***
Girder 2	0.95	2.42	2.80	3.21	***2.51***
Girder 3	0.95	2.69	3.11	3.57	***2.89***
Girder 4	0.95	3.61	4.18	4.81	***3.31***
Girder 5	0.95	2.52	2.92	3.36	***2.57***
Girder 6	-0.22	1.93	2.23	2.56	***NA***

Modified Load Rating Procedure for the MP28.9 Bridge

Based on the experimental results and an examination of the FE model, the following approaches to modifying the conventional load rating analysis of the MP28.9 Bridge are proposed:

- Dead load stresses from the FE model should be used when calculating the load rating. This is particularly true for the exterior girders as the single-line girder approach produces dead load actions for these girders that are close or even greater than their capacities.
- An impact factor of 1.15 (the largest measured) should be used for vehicles that will not be forced to crawl across the bridge. For vehicles that will be forced to crawl across the bridge, and impact factor of 1.00 should be used.
- A live load distribution factor of 0.35 should be used for each girder, which is larger than the largest distribution factor observed or simulated. In addition, this distribution factor would conservatively produce 50% greater live load actions than computed by the simulation model for the five construction vehicles considered.

This procedure should not be used for vehicles that have axle spacings and widths that are more compact that the test vehicle (standard two-rear axle dump truck). This caveat is needed as extremely concentrated forces could potentially have to be modeled using distribution factors larger than 0.35. In these cases the precise axle loads and spacings should be simulated using the FE model.

Applying the modified approach for each of the construction vehicles considered produces the rating factors shown in Tables 16 and 17 for interior and exterior girders, respectively.

Table 17 – Modified Rating Factors for overload vehicles – interior girder

Interior Girder	Dead Load Stress from Model (ksi)	Overload Vehicles				
		C-4-108	C-5-135	OT-3-70	OT-4-78	OT-5-100
Trans 1	23.825	1.23	0.98	1.81	1.65	1.29
Trans 2	14.1	4.03	3.21	5.93	5.42	4.24
Trans 3	16.875	2.94	2.34	4.3	3.93	3.08
Trans 4	12.35	5.13	4.08	7.48	6.85	5.37
Trans 5	12.625	4.85	3.85	6.97	6.41	5.03

Table 18 – Modified Rating Factors for overload vehicles – exterior girder

Exterior Girder	Dead Load Stress from Model (ksi)	Overload Vehicles				
		C-4-108	C-5-135	OT-3-70	OT-4-78	OT-5-100
Trans 1	25.7	1.06	0.85	1.57	1.43	1.12
Trans 2	16.6	3.5	2.79	5.15	4.7	3.68
Trans 3	18.8	2.68	2.13	3.92	3.58	2.8
Trans 4	12.3	5.32	4.23	7.78	7.11	5.58
Trans 5	13.5	5.21	4.14	7.5	7.18	5.41

Conclusions and Recommendations

Based on the activities outlined in the previous sections, the following conclusions are drawn:

- The measured neutral axis locations are above the fully composite values calculated in the conventional load rating analysis showing the bridge does act compositely. The discrepancies are due to assuming nominal material properties, neglecting the stiffness contribution of the asphalt overlay, and applying conservative estimates of effective width.
- The experimental distributions factors were approximately half of those prescribed by AASHTO and were consistent with those extracted from the FE model of the bridge.
- The retrofit plate was found to actively resist live load, with measured stresses of the same magnitude as the parent girder. It was also found to be active over the length in which measurements were taken (approximately 7 ft closer to the support than the transition).
- Based on the observed responses, the developed FE model was shown to be both conservative and representative of the behavior of the MP28.9 Bridge.
- All girders of the MP28.9 Bridge have rating factors above 1.0 for the HL-93 Live Load.
- Using the validated FE model, the bridge was found to rate for the five construction vehicles considered, if they are forced to crawl across the bridge. If an impact factor of 1.33 is used, then Girder 6 does not rate for the C-4-108 vehicle, but all other girders do rate.

- It is recommended that all heavy construction vehicles that are permitted to cross the bridge be forced to crawl in the center lane to minimize dynamic amplification and to maximize the transverse distribution of the load.

Disclaimer

Any opinions, findings, and conclusions expressed in this report are those of the authors, and do not necessarily reflect those of Drexel University.